

Study on Upper Troposphere / Lower Stratosphere Sounding

ESA Contract No.: 12053/97/NL/CN

Draft Final Report

Version: 1 / Revision: 0 (Draft)

W.J. Reburn, R. Siddans, B.J. Kerridge
Rutherford Appleton Laboratory, Chilton, Didcot, U.K.

J. Wohlgemuth, S. Bühler, J. Urban, A. von Engel, K. Künzi
Institute of Environmental Physics, University of Bremen, Germany

D. Feist, N. Kämpfer
Institute of Applied Physics, University of Berne, Switzerland

H. Czekala,
Meteorological Institute, University of Bonn, Germany

May 29, 1998

Contents

I Investigation of Instrument Parameters and Cloud-Free Measurement Capabilities	1
1 Introduction	3
2 FM and RM development	5
2.1 Introduction	5
2.2 Forward Model Development (WP1110)	5
2.2.1 RAL	5
2.2.2 IFE	8
2.2.3 IAP	9
2.2.4 University of Oxford	9
2.3 Selection of Scenarios	10
2.4 Intercomparison of Cloud-Free FMs (WP1120)	15
2.4.1 General considerations	15
2.4.2 Results	18
2.4.3 Conclusions	22
2.5 Retrieval Model Development (WP1210)	23
2.5.1 Theory	23
2.5.2 Overview of the RAL RM	29
2.5.3 IFE RM	31
2.6 Intercomparison of RMs (WP1220)	32
2.6.1 Scenario for the intercomparison	32
2.6.2 Results	33
2.6.3 Conclusions	59
2.7 Review of Spectral Line Selection after FM/RM Intercomparison	59
3 Investigation of Instrument Parameters	71
3.1 Spectral Parameters	71
3.1.1 Selection of “Baseline” Bandwidths	71
3.1.2 Comparison of Different Bands	73
3.1.3 Selection of “Optimised” Bandwidths	89
3.1.4 Selection of “Optimised” Frequency Resolution	89
3.1.5 Retrieval Sensitivity to Frequency Shift	103
3.2 Antenna Parameters	103
3.2.1 Optimisation of Retrieval and Forward Model Parameters	103
3.2.2 Beamwidth: Optimal Estimation Simulations	104
3.2.3 “Infinitesimal” Beamwidth	118
3.2.4 Global Fit Simulations	123

3.2.5	Beamwidth: Global Fit Simulations	123
3.2.6	Antenna Pattern: Optimal Estimation Simulations	130
3.2.7	Antenna Pattern: Global Fit Simulations	144
3.2.8	Knowledge of Static Antenna Pattern	157
3.2.9	Expansion/Compression of Effective Pattern During Measurement	171
3.2.10	Sensitivity to Horizontal Humidity Excursions Below the Tangent Range	171
3.2.11	Sensitivity to Horizontal Humidity Excursions Below Tangent Range for Different Antenna Patterns	173
3.3	Pointing Parameters	186
3.3.1	Linear Mapping of Bias and Drift Errors	186
3.3.2	Linear Mapping of Pointing Jitter	199
3.3.3	Demonstration through Non-Linear Band B Retrieval Simulation of Recovery from a 2km Pointing-Bias	212
3.3.4	Pointing/Temperature Information Specific to the O ₂ Line in Band B and Assessment of Random and Systematic Errors on Pointing Retrieval	212
3.4	Radiometric Parameters	220
3.4.1	Initial Simulations with Linear Mapping	220
3.4.2	Linear Mapping of Slope on Side-Band Response	246
3.4.3	More Realistic Linear Mapping of AOS Discontinuities	259
3.5	Linear Mapping at High Spectral Resolution for Band E	272
3.6	Further Simulations to Investigate H ₂ O Retrieval Sensitivities	275
3.6.1	Sensitivity to <i>A Priori</i> Uncertainty of Errors in Band C Retrieved Upper Tropospheric H ₂ O	275
3.6.2	Non-linear Retrieval Simulations for Band C H ₂ O	279
3.6.3	Attribution of “out-of-Band” H ₂ O lines: sensitivity of Band A and C H ₂ O retrievals	283
3.7	Indicative Random and Systematic Error Budgets on Retrieved Profiles	292
3.8	Options for Limb-Scan and Calibration Scenarios	343
4	Retrieval Simulations for a 2-D Cross-section	345
4.1	Synthesis of Measurements	345
4.2	Initial Modifications to the Retrieval Model	346
4.3	Retrieval Simulations and Current Results	346
5	Retrieval Simulations for Combined Bands	353
5.1	Objectives	353
5.2	Combining Information from Multiple Bands	353
5.2.1	O ₃	354
5.2.2	H ₂ O	354
5.2.3	T & Scan-Offsets	354
5.2.4	HNO ₃	354
5.2.5	N ₂ O	355
5.2.6	CH ₃ Cl	355
5.2.7	HOCl	355
5.2.8	ClO	355

5.2.9	BrO	355
5.2.10	Summary	355
5.3	Retrieval of Inter-Band Co-registration Errors	369
6	Temperature retrieval from non-uniform gases	373
6.1	Theoretical background	373
6.1.1	Saturation effects	373
6.1.2	Lines with different temperature dependence	374
6.1.3	Band Investigations	374
6.2	Retrieval simulations	376
6.2.1	Retrieval from non-uniformly mixed gases	376
6.2.2	Retrieval from oxygen lines revisited	379
6.2.3	Absorption offset nonlinearity	382
7	Comparison of Retrieval Capabilities for Equatorial, Mid-latitude and Polar Conditions	397
8	Conclusions and Recommendations	411
8.1	Forward and Retrieval Models and Approach to Error Analysis	411
8.2	Instrument Specification	412
8.2.1	Spectral Parameters	412
8.2.2	Geometric Parameters	413
8.3	Measurement Capabilities	414
8.3.1	Assumptions	414
8.3.2	Pointing and Temperature Profile Retrieval	415
8.3.3	Constituent Profile Retrieval	416
8.3.4	Multi-band Retrievals	417
8.3.5	Horizontal Structure in the Troposphere	417
8.4	Summary of Main Conclusions and Recommendations	417
8.5	Further Work	418
8.5.1	Scientific Studies	418
8.5.2	Technology Development	419
II	Investigation of MAS Capabilities to Retrieve Upper Troposphere Humidity	421
9	WP1230: MAS UTH retrievals	423
9.1	Introduction	423
9.2	Measurement technique	423
9.2.1	Retrieval of atmospheric profiles	425
9.2.2	Implementation of the forward model	427
9.3	Retrieval simulations	428
9.4	Comparison with measured data	429
9.5	Conclusions	432

10 MASTER WP-2150:

The potential impact of clouds	437
10.1 Overview	437
10.2 Review on high altitude cloud climatology	438
10.2.1 Introduction	438
10.2.2 SAGE II global cloud occurrence frequency	439
10.2.3 Cloud horizontal extent	442
10.2.4 Cloud top pressures	443
10.3 Cirrus cloud microphysics	445
10.4 Parametrisation of representative clouds	447
10.4.1 Horizontal and vertical extent	447
10.4.2 Cloud top altitudes	448
10.4.3 Cirrus particle size distributions	448
10.5 The multiple-scattering forward model	450
10.6 Validation of the SHDOM implementation	452
10.6.1 Introduction	452
10.6.2 Investigation of Available Distributions	452
10.6.3 IAP Forward Model BEAM	453
10.6.4 Results of zenith comparisons	454
10.6.5 Limb sounding simulations with BEAM	454
10.6.6 Conclusions	456
10.7 Broadband Cloud Simulations	456
10.8 Profile Retrieval in the Presence of Clouds	458
10.8.1 Variation of the absorption offset a priori error	460
10.8.2 Clear Sky Calculations	461
10.8.3 Cirrus Cloud 1 Calculations	462
10.8.4 Cirrus Cloud 2 Calculations	463
10.8.5 Cirrus Cloud 3 Calculations	463
10.8.6 Cirrus Cloud 4 Calculations	465
10.8.7 Cirrus Cloud 5 Calculations	465
10.8.8 Results	466
10.9 Assessment of irregular crystal shape	467
10.9.1 Theory	468
10.9.2 Application to off-nadir directions	469
10.9.3 Numerical calculations	469
10.9.4 Conclusions	471
10.10 Summary and conclusions	477
A Cloud retrieval plots	479
A.1 Band E, cirrus 2	479
A.2 Band A, cirrus 3	483
A.3 Band B, cirrus 3	487
A.4 Band C, cirrus 3	491
A.5 Band D, cirrus 3	495
A.6 Band E, cirrus 3	499

A.7	Band A, cirrus 4	503
A.8	Band B, cirrus 4	507
A.9	Band C, cirrus 4	511
A.10	Band D, cirrus 4	515
A.11	Band E, cirrus 4	519
A.12	Band A, cirrus 5	523
A.13	Band B, cirrus 5	527
A.14	Band C, cirrus 5	531
A.15	Band D, cirrus 5	535
A.16	Band E, cirrus 5	539

spectrum in band C. In band C most of the water vapor information comes from the slope which is strongly affected by clouds. In band A the cloud generates an offset rather than a slope.

The sensitivity to cloud contamination is increased by simultaneous temperature retrieval since temperature enters the calculation of all other retrieval molecules. Therefore, band B is strongly affected by the cloud. Temperature profiles for the altitude region of cirrus clouds are available from numerical weather prediction models, offering the opportunity to identify cirrus cloud contamination by comparison of retrieved to numerical profile. The retrieved absorption offsets could also be employed for this purpose.

The influence of clouds decrease towards higher frequencies because the opaque altitude region of the spectra moves to higher tangent altitudes. Therefore clouds at low altitudes are already inside of the opaque region.

The presence of a cloud is a major problem for the retrieval which can not be compensated by the introduction of an absorption coefficient offset. The cloud effects vary with altitude and size distribution (see section 10.7), leading to either an overestimation or underestimation in the observed brightness temperature. Therefore the introduction of an additional absorber in the absorption coefficient offset does not compensate scattering effects. There are probably two main reasons for this. Firstly, scattering is sufficiently strong to make the treatment of the cloud as an absorber inadequate. Secondly, the cloud introduces a horizontal inhomogeneity, because its horizontal extent is limited. This means that the cloud is — at least partly — missed by the antenna beam for tangent altitudes below the cloud altitude. Hence, even if the cloud itself could be treated as an absorber there would be an inconsistency. Consequently, the retrieval can calculate absorption coefficient offsets which are below the true value (see section A.4), introducing less absorption in the presence of a cloud!

On the other hand, concerning the possibility of retrieving cloud characteristics, it has to be concluded that is not easily possible to determine the properties of the cloud from the limb scan measurement. Different clouds lead to different effects in the retrieved profiles and the effects are related to the cloud properties and the altitude of the cloud in a complicated and very non-linear way. The Limb sounding geometry is therefore not as suitable as the Nadir geometry for cloud retrievals.

10.9 Assessment of irregular crystal shape

Multiple scattering of microwave radiation in ice clouds consisting of nonspherical particles is currently approximated by means of Lorenz-Mie theory. Therefore spherical particles with an equivalent radius must be assumed. Radiative transfer is calculated by a one-dimensional model that operates along the one-dimensional limb path. The objective of this working package is to find out if these approximations are sufficient in describing the effects of cirrus clouds on microwave radiation emerging from the atmosphere in limb directions.

Investigations on this problem require microwave scattering calculations with nonspherical particles that have a fixed orientation. The Meteorological Institute at the University of Bonn (MI) operates a radiative transfer model that is able to account for nonspherical particle shapes in microwave radiative transfer. Recent studies at MI have shown the importance of the knowledge of particle shape on one hand and the consideration of

anisotropic radiation (directional variation) on the other hand.

10.9.1 Theory

The influence of particle shape on radiative transfer is due to a different scattering and absorption behaviour. When considering these effects we are dealing with polarized radiation and therefore have to use a radiative transfer equation that takes into account that scattering, extinction and emission are different for all polarization states and that mixing between polarization components is possible.

Polarized microwave radiative transfer

In microwave radiative transfer the state of polarization is described by the four component Stokes vector $\bar{\mathbf{I}} = (I_v, I_h, U, V)$. From the electric field components of a polarized wave E_l and E_r the Stokes vector can be defined as

$$(10.6) \quad \bar{\mathbf{I}}' = \begin{pmatrix} I_v \\ I_h \\ U \\ V \end{pmatrix} = \begin{pmatrix} |E_v|^2 \\ |E_h|^2 \\ 2\text{Re}(E_v E_h^*) \\ 2\text{Im}(E_v E_h^*) \end{pmatrix}.$$

Considering nonspherical particles with a fixed orientation the vector equation of radiative transfer has to be used:

$$(10.7) \quad \cos \theta \frac{d\bar{\mathbf{I}}(z, \theta, \phi)}{dz} = - \overbrace{\bar{\sigma}_e(z, \theta, \phi)}^{\text{extinction matrix}} \bar{\mathbf{I}}(z, \theta, \phi) + \overbrace{\bar{\sigma}_a(z, \theta, \phi) B(T(z))}^{\text{emission vector}} + \int_0^{2\pi} \int_0^\pi \underbrace{\bar{\mathbf{P}}(z, \theta, \phi; \theta', \phi')}_{\text{phase matrix}} \bar{\mathbf{I}}(z, \theta', \phi') \sin \theta' d\theta' d\phi'.$$

In this equation the interaction parameters for extinction, emission and scattering depend on frequency, complex refractive index, size, shape, orientation of the nonspherical particle, direction of incidence and the direction of propagation, which is denoted by (θ, ϕ) .

Extinction and scattering both lead to mixing between the polarization components. In addition, the emission by nonspherical particles is polarized [Tsang *et al.*, 1985]. So the restriction to intensity only in microwave radiative transfer calculations (even with averaged phasefunctions and extinction coefficients) will not be correct. This limitation to intensity is also not sufficient when only Lorenz-Mie theory is used to calculate the effects of multiple scattering, because multiple scattering is known to produce polarization effects [Liu and Simmer, 1996].

Method of comparison

The comparison of results obtained with Lorenz-Mie theory and results depending on full nonspherical scattering theory is difficult. One has to define the equivalent ensemble of spheres that is compared with the ensemble of nonspherical particles. There are different approaches to this task and each of them has its own limitations. Defining an effective

diameter using an equivalent projected area of a particle neglects the effect of the particle's volume, which is important in the single scattering calculation. The following calculations use an effective radius defined by equal volumes of spherical and nonspherical particles. For all methods the size parameter in the case of large aspect ratios of the scattering particle is underestimated: Because spheres have a minimum radius per unit volume a needle- or plate-like crystal will lead to an equivalent drop size that is much smaller than the largest dimension of the nonspherical crystal.

10.9.2 Application to off-nadir directions

The radiative transfer code produces reliable results for plane parallel atmospheres and angles between nadir and 85° zenith angle. Closer to the horizontal the results become less accurate due to resolution effects: In each hemisphere the angle which is closest to the horizontal represents the interval up to 90° and therefore produces poor results, but for all other angles the results are reliable. A set of 16 angles per hemisphere is chosen with the last seven angles close to the horizontal: 79° , 83° , 85° , 86° , 87° , 88° , and 89° . This angle selection scheme results in an increased resolution along the tangent direction, reducing the stepwise transition between upwelling and downwelling radiation in transparent atmospheres.

This vector radiative transfer model is not able to produce correct results for limb-viewing geometry, which requires spherical geometry. Tangent directions in a horizontal infinite model will lead to infinite optical path lengths, resulting in infinite total optical thickness. But the sensitivity of intensity and polarization at angles close to the horizontal can be studied in order to get an impression of the effects to be expected for limb-sounding.

This assumption is based on the fact that along the limb path between the tangent point and the sensor all radiation is emerging in upward directions from the atmospheric plane parallel layers. So the effects observed close to the horizontal, but in upward directions, give a good indication about the relevant processes.

10.9.3 Numerical calculations

The one-dimensional radiative transfer model

The calculations presented in this report were carried out with the microwave radiative transfer model MWMOD developed by C. Simmer [Simmer, 1994] and recently extended to nonspherical scattering by H. Czekala [Czekala and Simmer, 1998],[Czekala et al., 1998]. The model uses plane parallel layers and an arbitrary set of discrete zenith angles to describe the atmosphere and the radiation distribution within. The radiative transfer equation is solved with the successive order of scattering method, thus allowing multiple scattering. Absorption of gases is calculated with Liebe's MPM code [Liebe et al., 1993b]. Interaction parameters for extinction, emission and scattering are calculated with Lorenz-Mie theory when considering spheres. For single scattering parameters of nonspherical particles we use the T-Matrix code from Mishchenko [Mishchenko et al., 1996] to calculate the complex amplitude scattering function. From this amplitude scattering function the absorption vector, extinction matrix and scattering phase matrix can be computed.

Using this single scattering model we are limited to rotational symmetric ellipsoids, also called spheroids. These particles have a fixed orientation with their rotational axis

aligned to the vertical. Profiles of temperature and water vapour used in our calculations are taken from a modified US-standard profile which has a temperature of 225 Kelvin at the tropopause.

Investigations on sensitivity to particle shape are carried out under very simplified conditions: Between 9 and 10 kilometers height an ice cloud was positioned. The particle size distribution is exponential with a maximum radius of 200 μm . The ice water content was fixed to 0.05 kg/m² and 0.3 kg/m², respectively. For nonspherical calculations the volume of the spherical crystals was converted to spheroids with a fixed aspect ratio of 5, so that the horizontal axis is five times larger than the vertical axis. This shape is used as an approximation of ice disks that are supposed to be found in cirrus clouds. The second shape which is used in this study is a spheroid with an aspect ratio of 0.2, having similarities with needle-like crystals with their longest axis oriented along the vertical. This is not meant as a realistic scenario, but as a help for interpretation of the results.

All calculations were carried out at the three frequencies of 200, 300 and 500 GHz, respectively, giving a rough coverage of the MASTER study spectral bands. A full frequency resolution would be impossible up to now because of limitations due to computing time.

Influence of shape on intensity

When comparing the clear sky case (Fig. 10.15) with the cloudy sky (Fig. 10.16) we obtain mainly a brightness temperature depression at all upward directions. Figure 10.17 shows this brightness temperature depression (defined as clear minus cloudy results) for spheres, the result for oblate spheroids (Fig. 10.18) looks quite similar.

A closer look at the difference of spherical and nonspherical calculations (Fig. 10.19) shows some remarkable results: Oblate ice crystals still lead to a brightness temperature depression, but a smaller one. The total intensity (compared to spheres) at upward directions close to the limb direction is increased, showing a decrease at nadir upward directions. This effect is enhanced with ice concentration in the cloud, as it is expected. As a general rule of thumb, this effect changes its sign when switching either to downward directions or to prolate crystal shapes instead of oblate (Fig. 10.20). The differences reach values of 10 to 20 Kelvin, depending on direction and frequency.

In the case of column-like (prolate) spheroids with vertical orientation we observe the largest differences in vertical direction, which is in contrast to the oblate spheroids, which show strong changes near tangent observation. This suggests two conclusions: At first the effects depend on the direction in which the largest dimension of the scattering particle is oriented. This may also be of some interest when ice-needles are considered which have their largest dimension set to the horizontal, which is closer to reality. This would result in transferring the results of nadir observations (with their large changes) to the tangent directions for needle-like crystals, too. Secondly we may say that the large differences in total intensity and their angular variation can be understood when looking at the polarization effects:

Nonspherical particles lead, in general, to a higher polarization ratio. But the extinction depends very strongly on direction and polarization. So the combination of polarizing the thermal emission from the atmosphere below and then adapting to the effect of polarization dependent extinction and absorption coefficients lead to results that can not be obtained with radiative transfer calculations restricted to total intensity.

Clear Sky

200.00 GHz Brightness Temperature / K

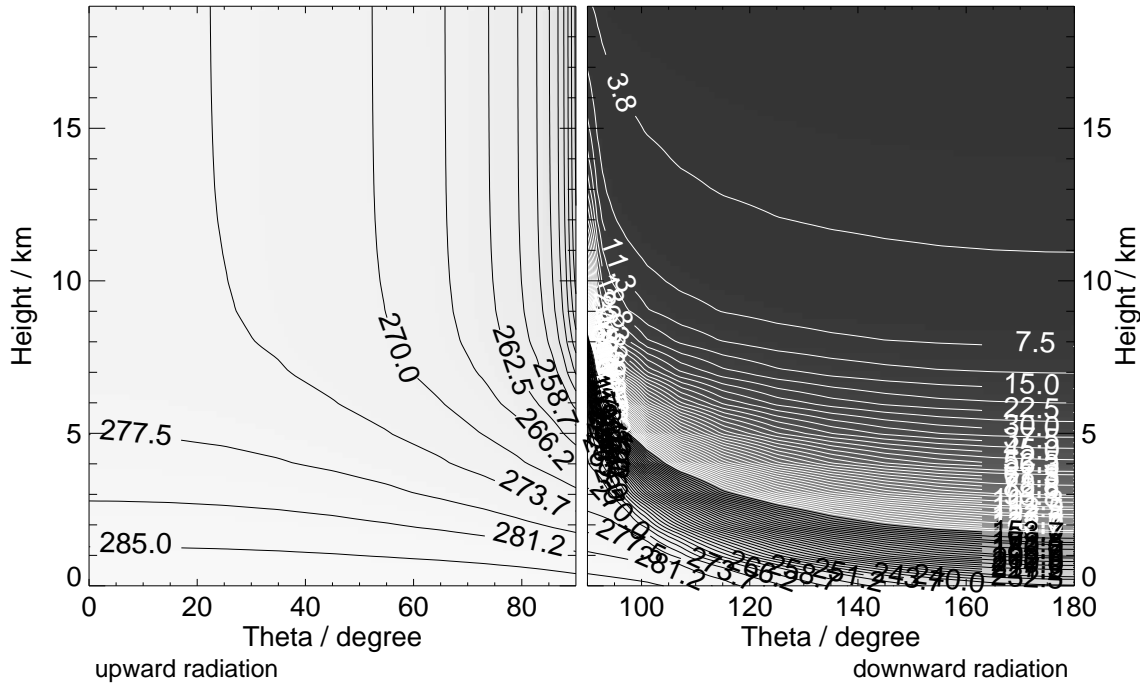


Figure 10.15: Distribution of total radiation intensity with vertical position and direction of propagation at clear sky conditions. Zero angle means nadir upward direction, 90 degree is the horizontal and 180 degree is directly downward.

Influence of shape on polarization

As pointed out some lines before the effect of nonspherical ice clouds on polarization is remarkable. The variable of interest is the polarization difference, which is defined as $(I_v - I_h)$.

Figure 10.21 shows the PD for oblate spheroids. In case of spheres the PD is close to zero, so we obtain a dominant effect of particle shape and orientation in this signal. Since simultaneously measurements in both, vertical and horizontal polarization, are not a feature of the MASTER instrument, the discussion of this topic is treated shortly. A detailed look on polarization effects can be found in *Czekala* [1998]. The main point which should be reported here is the fact that nonspherical shapes lead (in contrast to spheres) to high amounts (up to 20 Kelvin) of polarization difference, which will be positive or negative, depending on shape and orientation. This polarization signature strongly depends on the direction of observation and leads to a complex modeling scenario which can not be calculated with simple models geometries.

10.9.4 Conclusions

Although the geometry of our model is not able to calculate real limb-sounding geometry we showed that there are large error sources when radiative transfer is done by applying Lorenz-Mie theory to cirrus clouds. The effect of particle shape on both, intensity and polarization, is very complex. The variation of intensity with direction needs to be solved

Oblate Spheroid Cloud

200.00 GHz Brightness Temperature / K

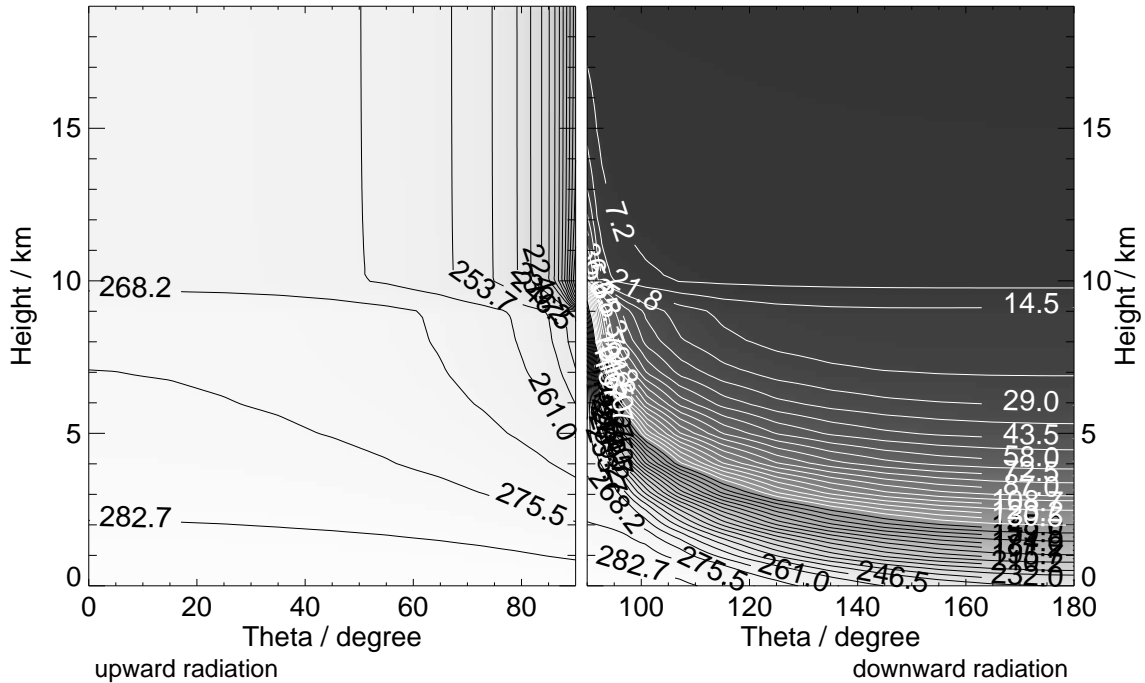


Figure 10.16: Distribution of total radiation intensity with vertical position and direction of propagation. This plot is for nonspherical (oblate) particles and IWC of 0.05 kg/m^2 .

with a model that uses more than only one dimension and a spherical coordinate system.

Furthermore it is essential that the state of polarization should not be neglected during the calculations, even if only the total intensity is of interest. In order to simulate the effects of scattering, extinction and emission correctly, the model should be able to handle nonspherical particles with a fixed orientation. This is of great importance because the final result will be very sensitive to these particle orientations together with the directional distribution of intensity close to the scattering volume and the polarization state of this intensity.

The nonspherical shapes used in this study are extreme examples and therefore produce strong effects. These simplifications enable us to study the basic processes in nonspherical microwave scattering, but there are more possible particle shapes to be investigated. Other shapes may lead to different scattering signatures. A particle of interest is the polycrystal introduced by A. Macke [Macke *et al.*, 1996], which is a good approximation to a mean cirrus particle in the visible region. Unfortunately, the microwave single scattering behaviour of such shapes can not be calculated with today's single scattering models.

Brightness Temperature Depression (Clear Sky - Cloud of Spheres)

200.00 GHz Brightness Temperature / K

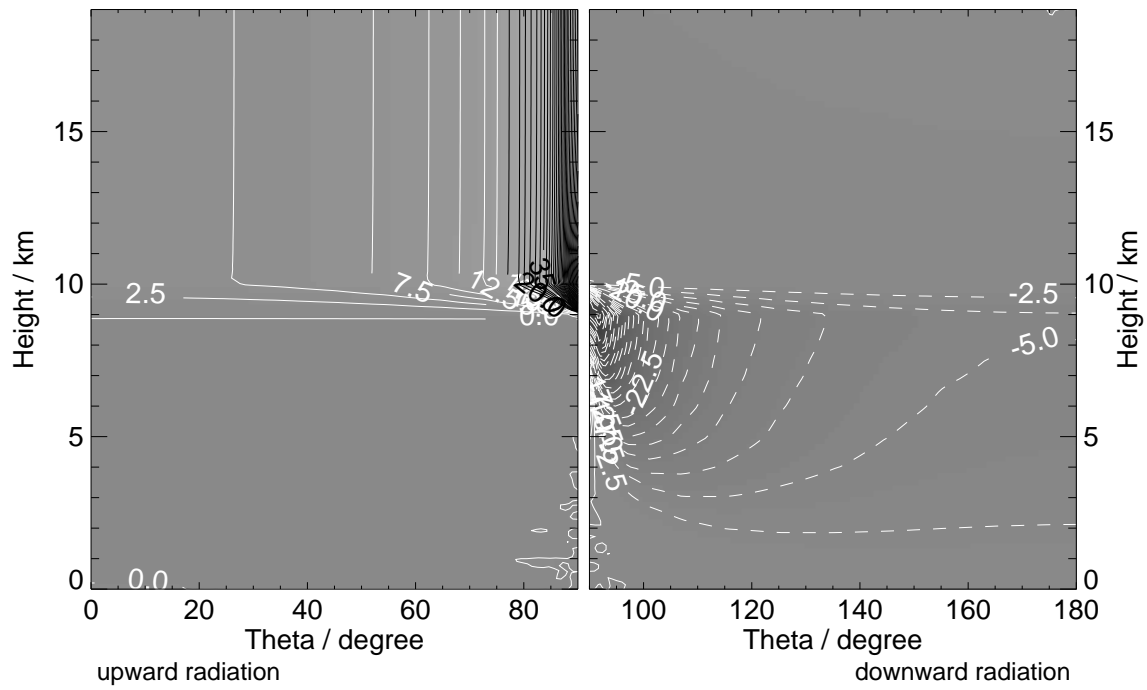


Figure 10.17: Brightness temperature depression (clear minus cloud) for spherical particles.

Brightness Temperature Depression (Clear Sky - Oblate Spheroid Cloud)

200.00 GHz Brightness Temperature / K

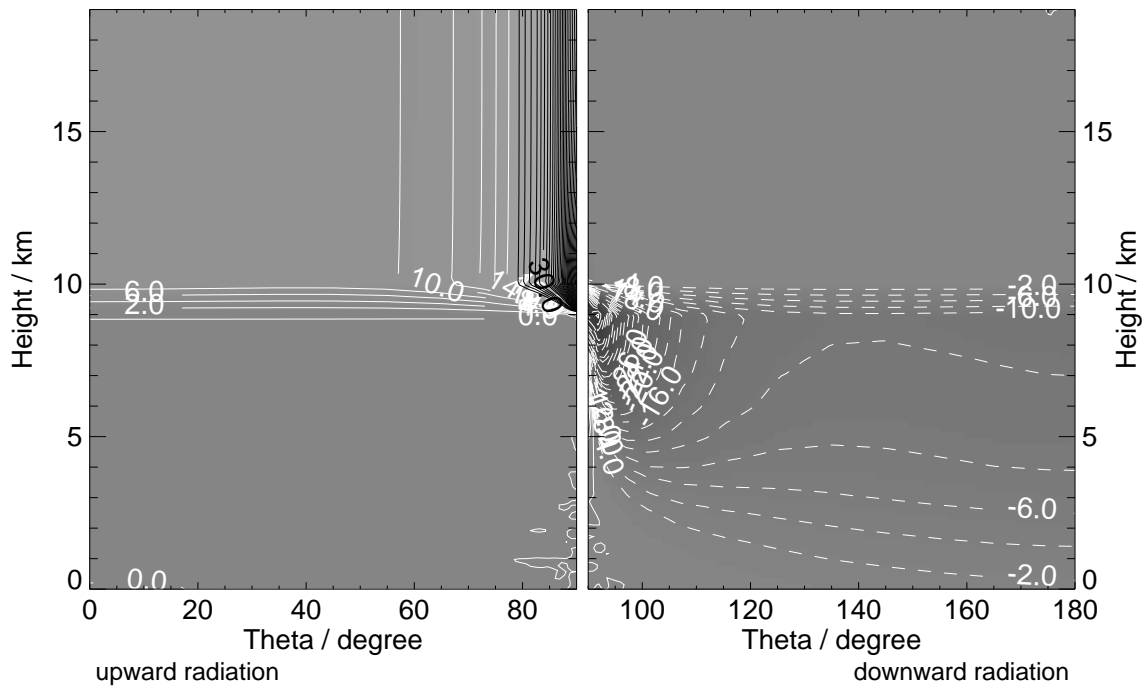


Figure 10.18: Brightness temperature depression (clear minus cloud) for oblate spheroids.

Difference (Oblate Shape - Spherical Shape)
200.00 GHz Brightness Temperature / K

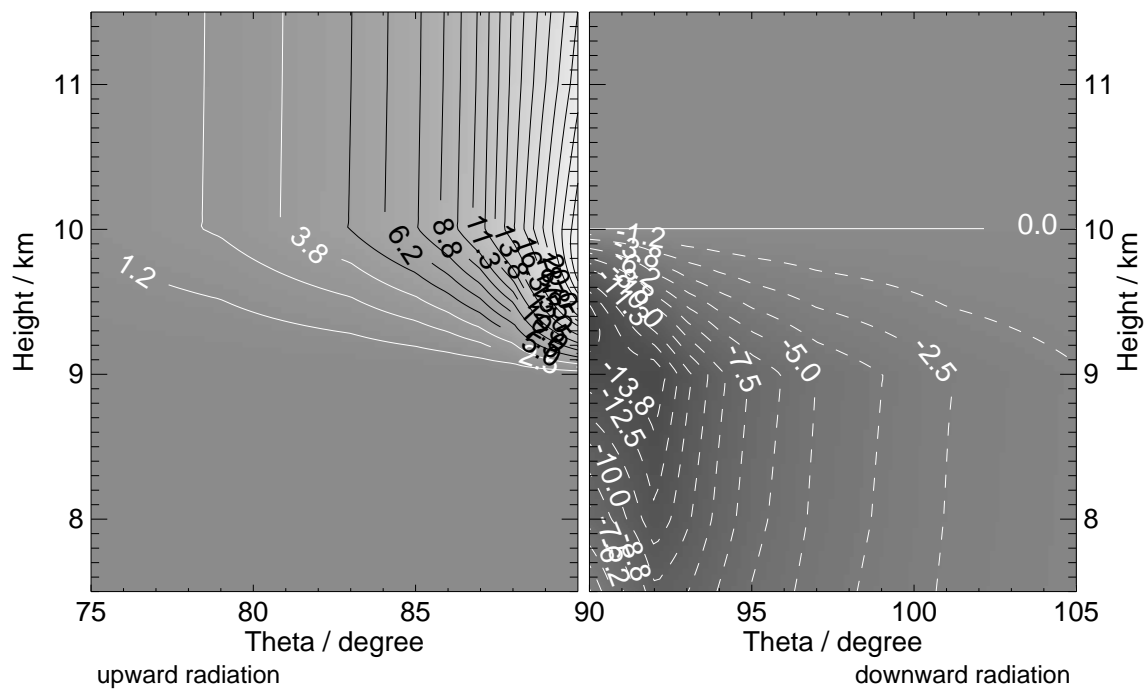


Figure 10.19: Difference between total intensity results obtained with oblate spheroids and spheres.

Difference (Prolate Spheroids - Spheres)
 200.00 GHz Brightness Temperature / K

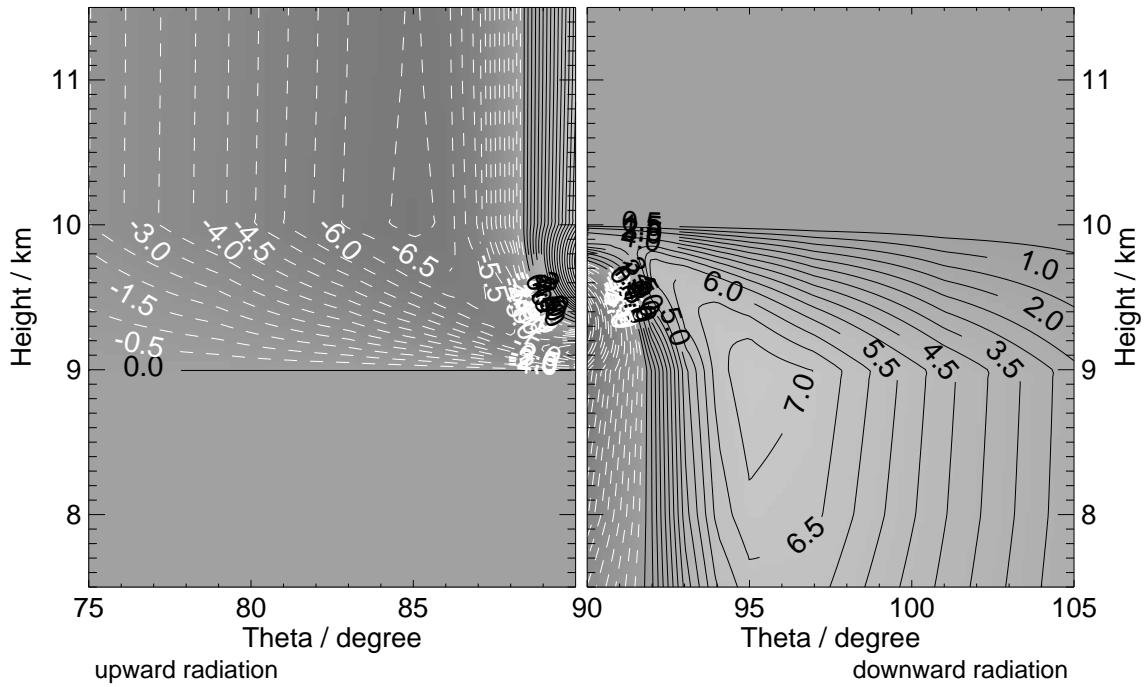


Figure 10.20: Difference between total intensity results obtained with prolate spheroids and spheres.

Oblate Spheroid Cloud
 200.00 GHz Polarization Difference / K

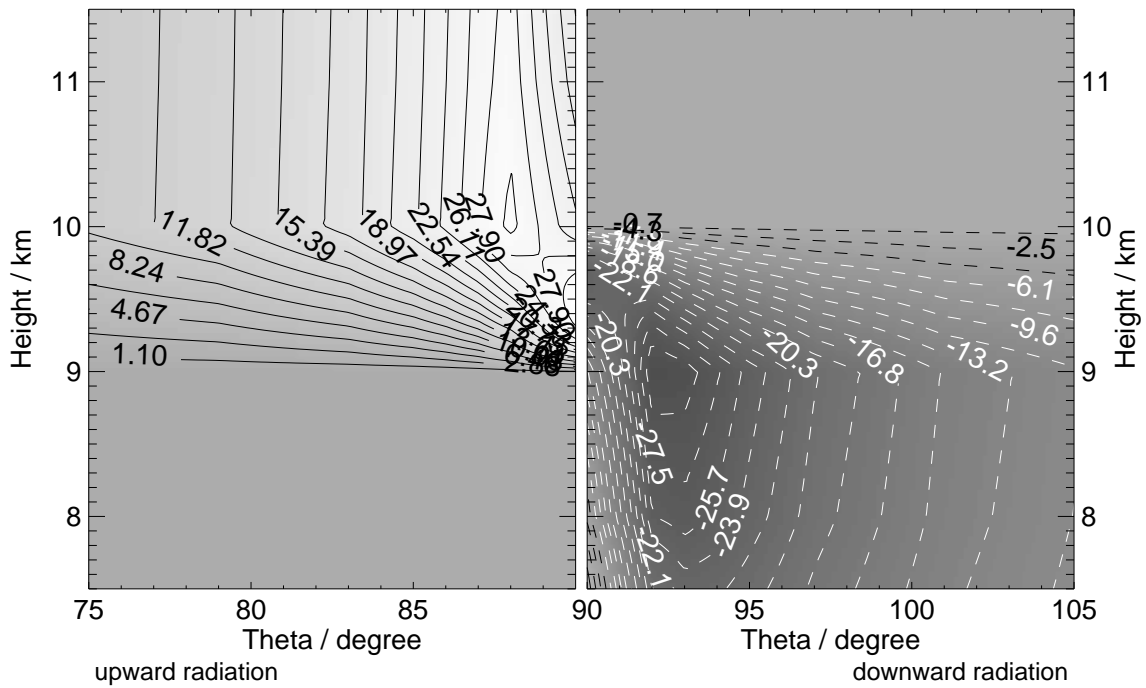


Figure 10.21: Polarization difference results obtained with oblate spheroids.

10.10 Summary and conclusions

Last but not least a summary of the chapter shall be given. The first part contained a review based on climatological cloud statistics of SAGE II and ISCCP with respect to cloud coverage, cloud altitudes as well as cloud vertical and horizontal extent. The published data allows an estimation of the abundance of cirrus clouds. According to SAGE II climatology the abundance of subvisual clouds is around 20 % at mid-latitudes and around 45 % in the tropics. The abundance of optically thick cirrus clouds is around 15 % at its maximum in the tropics.

The results of a number of field campaigns with respect to the microphysical properties of different types of cirrus clouds were summarized. This allowed to identify a representative set of typical cirrus clouds to be used for the retrieval simulations.

The state-of-the-art multiple-scattering radiative transfer model SHDOM was adapted to the present IFE radiative transfer model to allow realistic simulations of the effect of clouds for the MASTER spectral range and measurement geometry to be performed. The newly developed model is consistent with the IFE standard forward model in the clear sky case.

The radiative transfer in the presence of clouds was validated in up-looking geometry against the MWMOD multiple-scattering model of the University of Bonn and against the BEAM model of the University of Berne. The agreement with MWMOD is very good, but BEAM yields slightly lower brightness temperatures. This can be attributed to the fact that the BEAM model does not include scattering, only water extinction.

Broadband calculations in the limb-sounding geometry with the cloud radiative transfer model showed that brightness temperatures can be raised or lowered by the cirrus cloud, depending on cloud altitude and size distribution. Even at the same altitude, brightness temperatures can be raised by one cloud and lowered by another. The most important parameters to characterize the cloud are ice mass content and median mass equivalent sphere radius. The shape parameter α is relatively unimportant.

The cloud radiative model based on SHDOM was used to generate synthetic measurements for the set of test cases. These were then used to perform retrievals. The retrieval was affected by all clouds with a median mass equivalent sphere radius larger than 40 μm . Band A is less affected by clouds, retrieved profiles are within the given a priori errors whereas band C shows much stronger deviations from the true profile. This is due both to the different frequency regions and to the different properties of the water vapor spectrum in the two bands.

The sensitivity to cloud contamination is increased by simultaneous temperature retrieval since temperature enters the calculation of all other retrieval molecules. The temperature itself is strongly affected by the cloud. (Since temperatures for the altitude region of cirrus clouds are available from numerical weather prediction models, temperature — as well as absorption offsets — could be used for basic cloud detection, e.g., setting of a cloud flag.)

It was investigated whether the retrieval of an absorption coefficient offset can compensate the effect of cirrus clouds, but this is not the case. There are probably two main reasons for this. Firstly, scattering is sufficiently strong to make the treatment of the cloud as an absorber inadequate. Secondly, the cloud introduces a horizontal inhomogeneity that can not be ignored.

Concerning the possibility of retrieving cloud characteristics, it has to be concluded

that it is not easily possible to determine the properties of the cloud from the limb scan measurement. The best one can do is to detect the presence of a cloud from abnormal values of the absorption offset and the temperature profile.

The developed cloud radiative transfer model is limited to spherical particles. An assessment of the influence of particle shape on the modeled brightness temperatures was performed by MI Bonn. The result is that the effect of particle shape can not be neglected. This remains the largest uncertainty in the radiative transfer model with clouds. Nevertheless, the developed model is suitable for a first assessment of the cirrus cloud impact.

The most important conclusions with respect to the MASTER measurement capabilities are:

1. Cirrus cloud abundance is around 20 % at mid-latitudes, but up to 45 % in the tropics, according to SAGE II climatology.
2. Clouds can raise or lower the limb radiances and there is no easy rule of thumb for the effect of clouds on the measurement.
3. The retrieval of one or more absorption coefficient offset profiles can not compensate the cloud effect.
4. Cloud detection (setting of a cloud flag) should be possible from the measurement in most cases.
5. Retrieval of cloud properties is not very promising, the nadir geometry is better suited for cloud sensing.